Physica A 410 (2014) 628–640

Contents lists available at ScienceDirect

Physica A

journal homepage: www.elsevier.com/locate/physa

Dynamic range in small-world networks of Hodgkin–Huxley neurons with chemical synapses

C.A.S. Batista [a], R.L. Viana [a,*], S.R. Lopes [a], A.M. Batista [b,c]

[a] Department of Physics, Federal University of Paraná, Curitiba, Paraná, Brazil

[b] Department of Mathematics and Statistics, State University of Ponta Grossa, Ponta Grossa, Paraná, Brazil

[c] Institute for Complex Systems and Mathematical Biology, SUPA, University of Aberdeen, Aberdeen, Scotland, United Kingdom

HIGHLIGHTS

- The relationship between stimulus and response is a power-law within a given dynamic range.
- The dynamic range of sensory organs is larger than that of a single neuron.
- The exponent of the power-law depends on the coupling strength, network size and topology.

ARTICLE INFO

Article history:
Received 21 May 2014
Available online 3 June 2014

Keywords:
Small-world networks
Hodgkin–Huxley neurons
Dynamic range

ABSTRACT

According to Stevens' law the relationship between stimulus and response is a power-law within an interval called the dynamic range. The dynamic range of sensory organs is found to be larger than that of a single neuron, suggesting that the network structure plays a key role in the behavior of both the scaling exponent and the dynamic range of neuron assemblies. In order to verify computationally the relationships between stimulus and response for spiking neurons, we investigate small-world networks of neurons described by the Hodgkin–Huxley equations connected by chemical synapses. We found that the dynamic range increases with the network size, suggesting that the enhancement of the dynamic range observed in sensory organs, with respect to single neurons, is an emergent property of complex network dynamics.

1. Introduction

The quantitative relation between stimulus and response is perhaps the oldest problem in psychophysics [1]. Our experience suggests that this relation should be nonlinear: a linear relation would lead to an unbounded response, so overcoming the limited capabilities of our sensorial organs. Hence some form of response saturation should exist, limiting the response intensity to external stimuli. Weber and Fechner proposed, in the 19th century, that this relationship is logarithmic: the magnitude P of the response (sensation) related to a given stimulus of magnitude I is given by $P \sim \ln I$ [2].

In 1957 Stevens proposed a more general stimulus–response power-law relationship: $P \sim I^m$, where m is a positive response exponent that in most cases is less than 2 [1]. For example, for a sound pressure of 3 kHz tone (stimulus) the loudness response obeys Stevens' law with $m = 0.67$. However, the value of m may vary according the type of stimulus: the response to a vibrating plate, as captured by the sensorial organs at the finger, leads to different exponents of $m = 0.95$

* Corresponding author. Tel.: +55 41 99669606.
E-mail addresses: viana@fisica.ufpr.br, rlv640@gmail.com (R.L. Viana).

http://dx.doi.org/10.1016/j.physa.2014.05.069
0378-4371/

and 0.6, for a 60 Hz and 250 Hz vibration, respectively. Taste sensations have widely different values of m, namely 1.3, 1.4, and 0.8, when the stimulus is represented by sucrose, salt, and saccharine, respectively.

These power-law relationships between stimulus and response have upper and lower bounds due to anatomical and physiological limitations of the sensory organs. The dynamic range is the difference between the largest and the smallest values of the response intensity, expressed in decibels (dB). The human senses of sight and hearing have large values of the dynamic range, of 90 dB and 100 dB, respectively [3].

The diversity of values for the exponent m in Stevens' power law relationships, as well as the broad dynamic ranges exhibited by our senses are problems of current interest in computational neuroscience. Using models of complex neuronal networks one can investigate how the macroscopic features (namely, the power-law exponents and the dynamic ranges) are related to the microscopic behavior at the neuronal dynamics level. In the latter, the response of a neuron to a given stimulus can be represented by its firing rate, or the number of spikes it produces per unit time.

Those spikes are produced after injection of stimuli represented by an external input current, composed of a random sequence of stereotyped pulses with a given average input rate. Hence, from the microscopic point of view, the stimulus–response curve of a neuron would be its input rate-firing rate relationship, from which a power-law can be fitted with a given exponent. Likewise the dynamic range can be obtained from this power-law relationship by considering the response amplitude for which a power-law scaling holds.

Experimental evidence suggests that the dynamic range of a single neuron is substantially less than the dynamic range observed at the macroscopic level. As an example, in the case of olfactory system the receptor neurons have a dynamic range of the order of 10 dB, whereas the corresponding dendro-dendritic neural network in the glomeruli exhibits a dynamic range of about 30 dB [4,5]. Therefore the enhanced dynamic range at the macroscopic level can be regarded as a collective effect caused by the network structure.

Two basic mechanisms are thought to contribute to the dynamic range enhancement: (i) intrinsic variation of thresholds in a network of sensory neurons [6], and (ii) adaptation of each neuron to the statistics of the ambient stimuli [7]. Moreover, recently it was found that removing gap junctions (electrical synapses) causes a decrease in the dynamic range and an increase in the power-law exponent in Stevens' law [8]. This suggests that the enhancement of the dynamic range is possible by considering interactions among neurons through both electrical and chemical synapses.

On the other hand, it is known that electrical synapses are an important coupling mechanism of receptor cells of sensory systems [9,10]. The effect of electrical synapses has been investigated for neuronal networks using a cellular automaton model [11]. It has been observed that a maximal dynamic range is obtained at a non-equilibrium phase transition where self-sustained neuronal activity becomes stable [12–14]. The model of Kinouchi and Copelli included local connections only, and it was recently generalized by the addition of randomly chosen nonlocal connections [15,16]. However, the latter are not proper chemical synapses since the model did not take into account the fraction of open bond receptors, the reversal synaptic potentials, among other important effects.

Hence, in the present work we investigate the possibility of chemical synapses in the enhancement of the dynamic range and the changes in the exponent of the power-law relationship (sensitivity). The parameters that were considered in our investigation are the number of coupled neurons, the intensity of the coupling (maximum synaptic conductance), and the architecture of the neuronal network. One advantage of using a mathematical model is the possibility of including these effects separately. We used the Hodgkin–Huxley (HH) model to describe the neuronal dynamics [17], and the connection architecture is described by a small-world network, since the latter has properties shared by many networks of neuroscientific interest [18]. We restrict ourselves to chemical excitatory synapses, yet the model is flexible enough to allow for the inclusion of electrical synapses (gap junction) and also inhibitory connections. Recently a numerical investigation using HH neurons with inhibitory couplings has shown optimal properties near a bifurcation in the system dynamics [19].

This paper is organized as follows: in Section 2 we present the model used to describe both the neuronal dynamics based on HH equations and chemical synapses. Section 3 presents stimulus–response curves for a single HH neuron and discusses the scaling region and its characterization. The connection architecture, namely the small-world network structure, is described in Section 4. A detailed discussion of the stimulus–response curves for the coupled HH neurons in small-world networks is presented in Section 5. The last Section is devoted to our Conclusions.

2. Neuronal dynamics

In the following we consider the neuronal dynamics as described by the Hodgkin–Huxley model, which gives the time evolution of the membrane potential in terms of the interplay among voltage-gated potassium, sodium and leak channels [17]. Let $V_i(t)$ denote the membrane potential of the ith neuron (measured in mV) in a network with N units ($i = 1, 2, \ldots N$). The basic membrane equation is

$$C_m \frac{dV_i}{dt} = -I_{i,Na} - I_{i,K} - I_{i,L} + I_{i,ext} + I_{i,syn}, \tag{1}$$

where time is measured in ms; C_m is the specific membrane capacitance, measured in $\mu F/cm^2$; I_K and I_{Na} are ionic currents (actually current densities, measured in $\mu A/cm^2$) related to the ion channels embedded in the neuron membrane; I_L is the leak current, I_{ext} is the external input current; and I_{syn} is the current related to the synaptic connections with other neurons.

Table 1
Parameter values of the Hodgkin–Huxley model according to Ref. [20].

Membrane specific capacitance	$C_m = 1.0\ \mu\mathrm{F/cm^2}$	
Maximum specific conductances ($\mathrm{mS/cm^2}$)		
$\bar{g}_{Na} = 120$	$\bar{g}_K = 36$	$\bar{g}_L = 0.3$
Nernst (reversal) potentials (mV)		
$E_{Na} = 55$	$E_K = -72$	$E_L = -49$

The currents related to the ion and leak channels are given by conductance-based expressions [20]

$$I_{i,K} = \bar{g}_K n^4 (V_i - E_K), \tag{2}$$

$$I_{i,Na} = \bar{g}_{Na} m^3 h (V_i - E_{Na}), \tag{3}$$

$$I_{i,K} = \bar{g}_L (V_i - E_L), \tag{4}$$

where $\bar{g}_K$, $\bar{g}_{Na}$, and $\bar{g}_L$ are the maximum specific conductances (measured in $\mathrm{mS/cm^2}$) of the potassium, sodium, and leak channels, respectively, and the corresponding Nernst potentials of these channels are E_K, E_{Na}, and E_L (in mV). The numerical values of these parameters, to be used in the numerical simulations reported in this work, are given in Table 1.

The potassium activation variable (n), the sodium activation variable (m), and the sodium inactivation variable (h) – all non-dimensional quantities – satisfy the following differential equations [20]

$$\frac{\mathrm{d}n}{\mathrm{d}t} = -(\alpha_n + \beta_n) n + \alpha_n, \tag{5}$$

$$\frac{\mathrm{d}m}{\mathrm{d}t} = -(\alpha_m + \beta_m) m + \alpha_m, \tag{6}$$

$$\frac{\mathrm{d}h}{\mathrm{d}t} = -(\alpha_h + \beta_h) h + \alpha_h, \tag{7}$$

where the terms α_i and β_i ($i = n, m, h$), all measured in $(\mathrm{ms})^{-1}$, are given in terms of the membrane potential V by the following empirical relations [20]

$$\alpha_n(V_i) = 0.01 \frac{V_i + 50}{1 - \exp[-0.1(V_i + 50)]}, \tag{8}$$

$$\beta_n(V_i) = 0.125 \exp\left[\frac{V_i + 60}{80}\right], \tag{9}$$

$$\alpha_m(V_i) = 0.1 \frac{V_i + 35}{1 - \exp[-0.1(V_i + 35)]}, \tag{10}$$

$$\beta_m(V_i) = 4 \exp\left[\frac{V_i + 60}{18}\right], \tag{11}$$

$$\alpha_n(V_i) = 0.07 \exp\left[\frac{V_i + 60}{20}\right], \tag{12}$$

$$\beta_h(V_i) = \frac{1}{1 + \exp[-0.1(V_i + 30)]}. \tag{13}$$

The term $I_{i,syn}$ in Eq. (1) is the external current arriving at the ith neuron due to the synaptic coupling with other neurons. We will model the latter as chemical synapses: the $j = 1, 2, \ldots M$ pre-synaptic neurons release neurotransmitter molecules that diffuse along the synaptic cleft and form bonds with ligand receptors of the i the post-synaptic neuron. The fraction $r_j(t)$ of bond receptors of the jth pre-synaptic neuron obeys the following equation [21,22]

$$\frac{\mathrm{d}r_j}{\mathrm{d}t} = \left(\frac{1}{\tau_r} - \frac{1}{\tau_d}\right) \frac{1 - r_j}{1 + \exp(-V_j + V_0)} - \frac{r_j}{\tau_d}, \tag{14}$$

where V_j is the membrane potential of the jth pre-synaptic neuron, τ_r and τ_d are characteristic rise and decay times, respectively, and V_0 is a reversal potential.

The total synaptic current arriving at the ith post-synaptic neuron takes into account the pre-synaptic neurons which are actually linked with the post-synaptic one, in the following form [21,22]

$$I_{i,syn} = \bar{g}_c \sum_{j=1}^{N} a_{ij} r_j(t) (V_{i,syn} - V_j), \tag{15}$$

Table 2
Parameter values for the synaptic dynamics according to Ref. [22].

Characteristic times (ms)	
$\tau_r = 0.5$	$\tau_d = 8$
Reversal potentials (mV)	
$V_{syn} = 20$	$V_0 = -20$

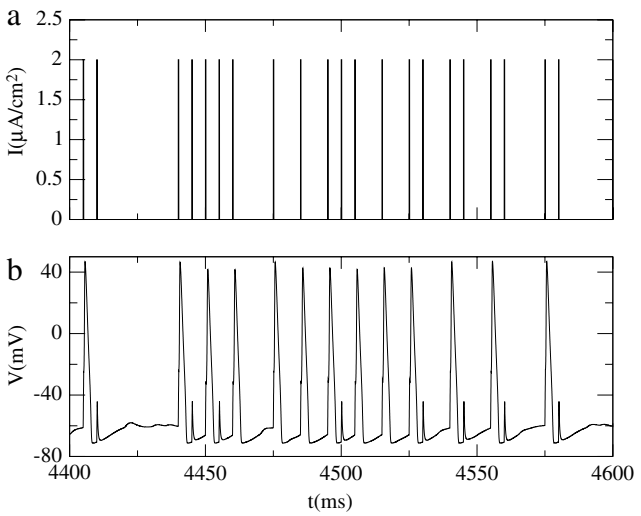

Fig. 1. (a) Electrical impulses and (b) spikes of a single neuron described by the Hodgkin–Huxley equations.

with $\bar{g}_c$ is the maximum specific conductance, measured in (mS/cm^2), a_{ij} are the elements of the synaptic adjacency matrix ($a_{ij} = 1$ if i and j are linked through a synapse, and $a_{ij} = 0$ otherwise), $V_{i,syn}$ is the synaptic reversal potential of the ith neuron, and $r_j(t)$ is the fraction of bond receptors (open synaptic channels) of the jth neuron. We assume, for simplicity, that all neurons have the same value of V_{syn}. The numerical values of the coupling parameters to be used in this work can be found in Table 2. The equations of the coupled model were integrated numerically using a fourth order fixed stepsize Runge–Kutta method.

3. Stimulus–response relationship for a single neuron

Sensory stimuli received by specialized organs are represented as trains of electrical impulses of short length that may be considered as stereotyped electrical events, or spikes. For example auditory stimuli are transduced by the cochlea into trains of spikes received by collections of neurons, each of them responding to a particular frequency [23]. The strength of those stimuli are coded not in the amplitudes of the spikes themselves, but in the time between spikes, according to a neural code based on the spike rate, or the number of spikes per time unit that influences a given neuron [24]. Such spikes, being electrical impulses, produce a current density that may be regarded as an input current I_{ext} in Eq. (1).

Another example is the sensory neurons of the retina, which respond to patterns of light displayed over small sections of the visual field. Even when subjected to constant light stimuli, those neurons spike spontaneously, such that the interspike intervals are different [25]. For the goldfish retinal neuron in culture under constant light and environmental conditions, there has been found that most of the interspike intervals are shorter than 20 ms, but a significant amount is much longer, on the order of 60–120 ms [26].

The histogram of interspike intervals is usually modeled as a Poisson distribution function. Poisson processes are characterized by the fact that the probability of firing a spike is independent of the firing activity at all other times, i.e. the interspike intervals are independent of the past spiking history. Bair et al. analyzed spike trains of neurons in visual area MT and found that, in about a third of the neurons, the interspike intervals were compatible with a Poisson process [27]. Let $\tau_k = t_k - t_{k-1}$ be the interspike time interval. Using a continuous-time distribution function, where $P(\tau)d\tau$ is the probability of finding an interspike interval between τ and $\tau + \mathrm{d}\tau$, we use a Poisson process for which

$$P(\tau) = 1 - \mathrm{e}^{-r\tau}, \tag{16}$$

where r is the input spiking rate.

In the following we will use a sequence of stereotyped electrical impulses corresponding to an external current density of $I = 2\,\mu\mathrm{A/cm}^2$, in such a way that the interspike interval satisfies a Poisson process with a given input rate r. Fig. 1(a) shows a train of spikes forming the external current I_{ext} acting on a single neuron described by the Hodgkin–Huxley model (1),

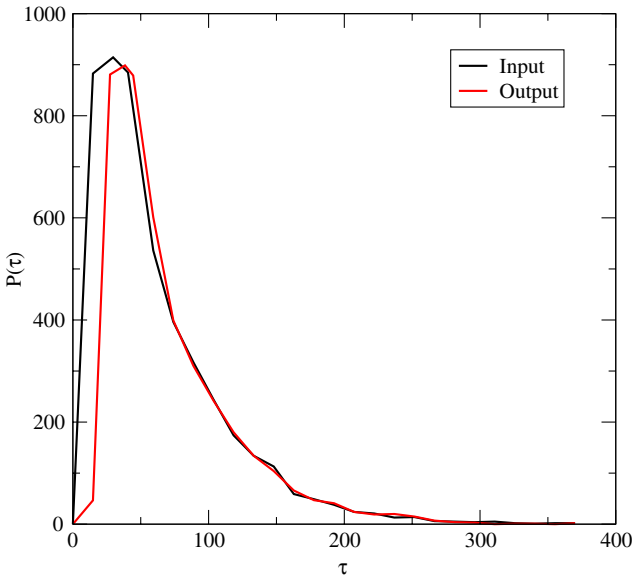

Fig. 2. Histogram of the interspike intervals for the stimulus (black line) and the response (red line) of a single neuron. (For interpretation of the references to color in this figure legend, the reader is referred to the web version of this article.)

followed by action potentials fired by the neuron [Fig. 1(b)]. When the input spike strikes the neuron while it is in a refractory period, the neuron will not produce an action potential (these frustrated responses are mini-spikes which will not be counted as actual spikes).

A numerical approximation to the Poissonian probability distribution function of the interspike intervals corresponding to the stimulus is shown in Fig. 2, with a similar distribution for the interspike intervals of the neuron response. The distributions have roughly the same range of values, the response peak being slightly displaced to the right with respect to the stimulus peak. This is because for small τ the stimuli hit the neuron more often when it is still in its refractory period and does not respond.

The response of a single neuron can be characterized by its firing rate, or the number of spikes per unit time. On varying the input rate r of the spike train corresponding to the stimulus it is possible to compute its firing rate F. Cortical neurons typically receive spontaneous input ranging from 10^4 to 10^5 spikes per second, corresponding to the range $r = 10$–$100\ (\text{ms})^{-1}$ for the input rate [28]. In peripheral sensory organs, however, the typical number of input spikes per second can be much fewer, with larger individual conductance changes, what corresponds to higher input rates in the 0.1–$1\ (\text{ms})^{-1}$ range [29]. We have considered, in numerical simulations, the latter regime so as to test the network response to the spike trains.

The numerical results shown in Fig. 3 reveal a sigmoid relationship between F and r: for very small input rates ($r \lesssim 0.01$) the response is nearly zero since a neuron spikes following the input signal it receives and, if these inputs have a too small input rate (too large interspike interval) the spiking rate is correspondingly tiny, what amounts to a minimum firing rate $F_{\text{min}} \approx 0$. Only for $0.01 \lesssim r \lesssim 0.1$ this response increases in a quadratic-like fashion.

For very large input rates ($r \gtrsim 1$) the neuron response is affected by the presence of a refractory time immediately after the neuron has fired a spike, because if a neuron is in its refractory period it will remain insensitive to further spikes. Hence there is a maximum firing rate, denoted $F_{\text{max}} = 0.2$ respectively. From this value we may estimate that the refractory period is $\sim 1/F_{\text{max}} = 5$ ms, what can be compared with the duration of the spike itself, which is ~ 1 ms. In fact, in the cellular automaton model of Kinouchi and Copelli time is discretized in 1 ms intervals, such that the spike duration is one unit and the refractory time is five units [12].

The response interval of a single firing neuron is hence $0.1 \lesssim r \lesssim 1$ and, within this range, the relationship can be fitted by a power-law $F \sim r^m$, where $m = 0.8$, just like in Stevens' law. Since these bounds are not strictly fixed, a practical way to give lower and upper bounds to this interval is to consider $F_{upper} = 0.9(F_{\text{max}} - F_{\text{min}})$ and $F_{lower} = 0.1(F_{\text{max}} - F_{\text{min}})$. Let us denote by r_{upper} and r_{lower} the input rates corresponding to F_{upper} and F_{lower}, respectively. The dynamic range is defined as

$$\Delta = 10 \log_{10} \frac{r_{upper}}{r_{lower}}, \tag{17}$$

and measured in decibels (dB). For a single neuron the dynamic range is smaller than of sensory organs. This discrepancy has led us to view the large dynamic range observed in experiments as a result of the network structure, what leads us to consider assemblies of neurons with a given connection architecture.

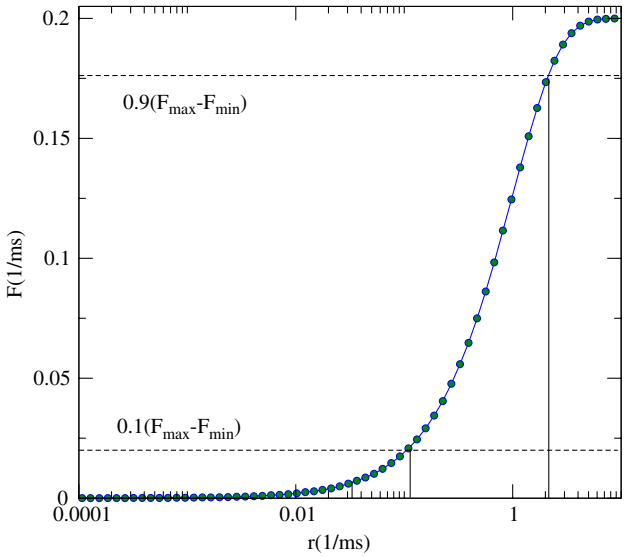

Fig. 3. (Color online) Firing rate of a single neuron *vs*. the input rate of a Poisson process of stereotyped spikes.

4. Network connectivity

In the brain, neurons are connected by synapses and form a complex network due to the large number of units ($\sim 10^{11}$ neurons) and the large connectivity (each neuron being connected to $\sim 10^4$ other ones, yielding $\sim 10^{15}$ connections) [30]. At a macroscopic level, one can describe a complex network by considering cortical areas as nodes, connected together by axonal fibers. The cortical areas are composed themselves of a large number of neurons, but in many instances they act as individual units, like when the brain is performing a given task or processing external stimuli [31]. In this paper, however, we will consider the microscopic level of description, where neurons are nodes, connected by synapses (links).

Using the language of graph theory, let us denote by N the number of nodes and K the total number of links. Two basic quantities used to characterize complex networks are their average path length L and the average clustering coefficient C [32]. The former is the minimum distance between pairs of nodes, averaged over all nodes in the network. The latter, roughly speaking, is the degree of overlap between neighborhoods of different sites. In other words, if we have a given node i connected to two other nodes j and k, C gives a probability that the nodes j and k are themselves connected [33].

A one-dimensional chain of nodes with nearest neighbor connections is an example of regular network, for which the average path length is $L \sim N$. If each node is connected with its 2ℓ nearest neighbors the corresponding clustering coefficient is [34]

$$C_{reg} = \frac{3(2\ell - 2)}{4(2\ell - 1)}. \tag{18}$$

On the other hand, random (Erdös–Renyi) networks are constructed connecting the N nodes with K links randomly chosen according to a uniform probability $p_{rand} = K/N(N-1)$ [35]. The average path length

$$L_{rand} \sim \frac{\ln N}{\ln[(K/N) - 1]}, \tag{19}$$

is relatively small, when compared with a regular lattice. The clustering coefficient $C_{rand} \sim (K/N)/N$ is also typically very small.

Small-world networks are characterized by values of L comparable to those of a random network ($L \sim L_{random}$) and a value of C much greater than of a random network ($C \gg C_{random}$) [36]. Hence small-world networks (with small L and large C) are in between two limit cases: regular networks (large L and C) and random networks (small L and C). It is customary to introduce the ratios [18]

$$\lambda = \frac{L}{L_{rand}}, \qquad \gamma = \frac{C}{C_{rand}}, \tag{20}$$

in such a way that, for a small world network, we can compute a merit figure ("small-worldness") [37]:

$$\sigma = \frac{\gamma}{\lambda} > 1, \tag{21}$$

in the sense that, the higher is σ for a network, the better it displays the small-world property.

One of the few neuroanatomic networks known in detail is the nervous system of *C. elegans*, which has $N = 279$ neurons connected by $L_{elec} = 514$ electrical (gap-junction) synapses and $L_{chem} = 2194$ chemical synapses [38]. The adjacency matrices for both synapses are different. For the electrical synapses there has been found that the path length and clustering coefficient are equal to $L = 4.52$ and $C = 0.21$, respectively. A random network constructed with the same number of nodes and links (corresponding to a probability $p_{rand} = 0.007$) would have path lengths and clustering coefficients equal to $L_{rand} = 4.0$ and $C_{rand} = 0.015$, respectively. Hence the ratios (20) are $\lambda = 1.13$ and $\gamma = 14$, such that the merit figure is $\sigma = 12.4$ indicates that this is indeed a small-world network [18]. A similar analysis, performed on the network of chemical synapses, yields a merit figure of $\sigma = 2.38$, which indicates that the small-world property still holds for it, although in a weaker sense.

In a macroscopic point of view, where cortical areas play the role of nodes and the links are axonal fibers, SW networks also appear, e.g. for the macaque and the cat [39]. For the macaque visual cortex, we have $N = 32$ cortical areas and $K = 305$ axonal connections, yielding an average path length of $L = 1.73$ and clustering coefficient of $C = 0.53$ [40,41]. After a comparison with a random network with the same number of nodes and links we have the ratios (20) equal to $\lambda = 1.04$ and $\gamma = 1.47$, yielding a merit figure of $\sigma = 1.41$ which suggests that the small-world property holds for this network. Similar conclusions are drawn for the macaque and cat whole cortex, both displaying the small-world property with $\sigma = 2.61$ and 3.22, respectively [31,42].

Another kind of networks of neuroscientific interest are functional networks, where cortex regions are the nodes, like in macroscopic neuroanatomic networks, but the links are provided by correlations between functional activity of these regions, are evidenced by various methods, like neuronographic data, human electroencephalography (EEG), functional magnetic resonance imaging (fMRI), etc. There is sound evidence that those functional networks display the small-world property [18]. These empirical findings suggest that a small-world network would represent a neuronal network (in a microscopic or macroscopic level) better than a random or regular network.

It is possible to obtain small-world networks from regular lattices following a procedure from Newman and Watts [34]: we start from a one-dimensional chain with connections between nearest neighbors and next-to-the-nearest neighbors. Then we add nonlocal shortcuts to randomly chosen nodes of this chain with a uniform probability p. These shortcuts are ultimately responsible for diminishing the path length in the network, whereas the nearest neighbors account for the large clustering coefficient displayed by small-world networks. There is also a procedure from Watts and Strogatz which, instead of adding new shortcuts, replug some of the local connections into non-local ones [36].

We constructed small-world networks according the Newman–Watts procedure described above, starting from a one-dimensional regular chain of N nodes, where each node is connected to its 2 nearest neighbors. The two parameters characterizing the network architecture to be used are the number of neurons N and the probability of nonlocal shortcuts p. The small-world property holds for a wide class of Newman–Watts networks, obtained with probabilities ranging from $p = 0.001$ to $p = 0.01$. Proceeding in this way we obtained a corresponding adjacency matrix a_{ij}. Since the probability p is typically small, this matrix is band-diagonal and presents sparse nonzero elements at both sides.

5. Stimulus–response relationship for coupled neurons

The behavior of coupled neurons is obtained by numerically solving the differential equations shown in Section 2, with the parameters given in Tables 1 and 2. We adopt random initial conditions and periodic boundary conditions, and the adjacency matrix was obtained as described in the previous Section.

The only model parameter we choose to vary in this work is the maximum specific conductance $\bar{g}_c$, which plays the role of the coupling strength. If the latter is zero the uncoupled neurons display uncorrelated spiking [Fig. 4(a)], what can also be observed by considering the corresponding raster plot [Fig. 4(c)], in which we plot the time instants in which the neurons fire a spike. As the neurons become coupled they tend to spike in roughly the same instants of time [Fig. 4(b)], yielding a correlated spiking activity that it is apparent in the corresponding rasterplot, forming a kind of "spiking wave" propagating along the network [Fig. 4(d)]. Such spiking waves have been also observed in a cellular automaton model [15].

When considering networks of coupled neurons, we apply the input spike train in all neurons simultaneously, what is a reasonable assumption given that we may think of our network as representing an assembly of sensory neurons receiving signals from specialized organs like cochlea or retina. The spiking train is composed of stereotyped events (spike) whose interval is taken from a Poisson distribution with input rate r. The stimulus intensity is input spiking rate r (which is the same for all neurons) and the response intensity is the firing rate F, averaged over the entire network.

The relation between F and r is observed to be of sigmoidal nature over five orders of magnitude of the stimulus, as illustrated in Fig. 5(a), where each curve is obtained using a different value of the coupling strength $\bar{g}_c$. We have used, as for the single neuron, the bounds of the scaling interval those values corresponding to 10% and 90% of the maximum firing rate (the minimum firing rate would not be suitable for this purpose since it depends on the coupling strength, whereas the maximum firing rate is practically constant). The maximum value of the firing rate ($F_{\max}$) is 0.2 irrespective of the coupling among neurons. This is because the maximum firing rate is determined by the time interval during which the neuron lies in the refractory period, which depends only on the neuronal dynamics (in our case, the Hodgkin–Huxley equations) and is thus independent of the coupling.

It is worthwhile mentioning that, even for uncoupled neurons [blue points in Fig. 5(a)] there is such a sigmoidal response curve, although the minimum value of the firing rate $F_{\min}$ is zero, just like for the single neurons, as expected. As the coupling

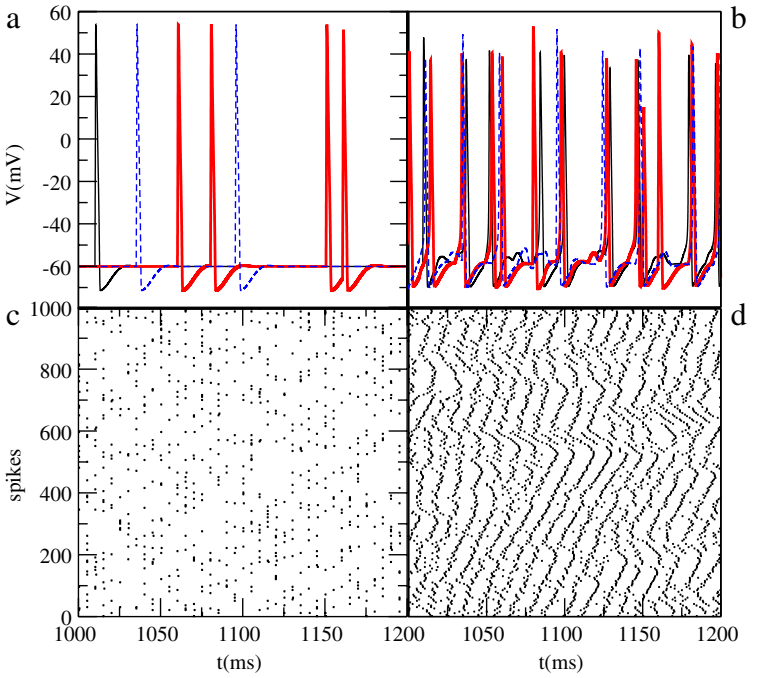

Fig. 4. (Color online) Time evolution of the membrane potential for a selected number of neurons when (a) $\bar{g}_c = 0$ and (b) $\bar{g}_c = 0.06$ mS/cm^2. (c) and (d) are rasterplots indicating the spiking neurons, corresponding to (a) and (b), respectively.

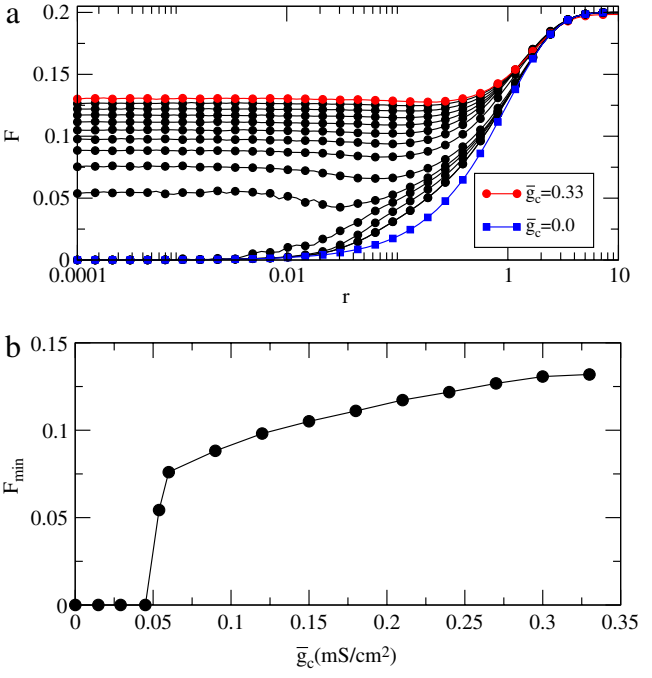

Fig. 5. (a) Firing rate *vs.* spike input rate for various values of the coupling strength, from 0.0 (blue line) to 0.33 (red line). (b) Minimum firing rate as a function of the coupling strength. We considered $p = 0.001$ and $N = 2000$. (For interpretation of the references to color in this figure legend, the reader is referred to the web version of this article.)

strength becomes nonzero the value of $F_{\min}$ increases. Actually its behavior with $\bar{g}_c$ resembles a phase transition, since $F_{\min}$ is zero (within the numerical precision) until $\bar{g}_c$ attains a critical value ∼0.045, after which $F_{\min}$ increases monotonically and appears to saturate at a value *circa* 0.13 [Fig. 5(b)].

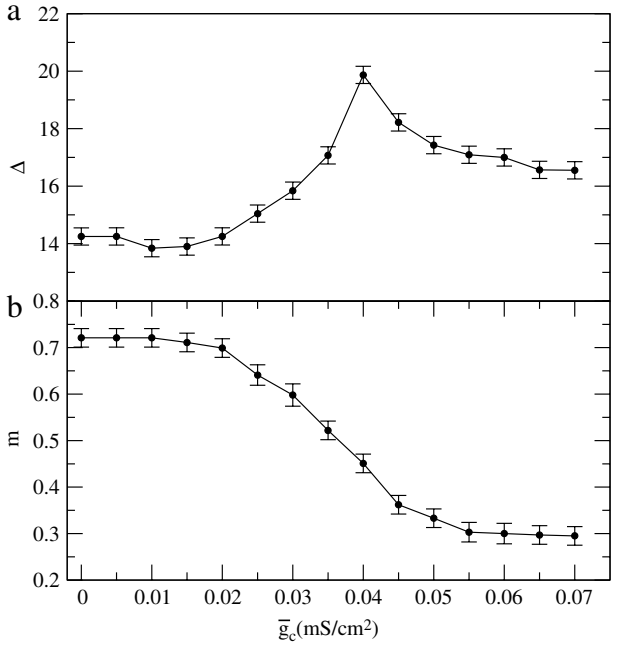

Fig. 6. (a) Dynamic range and (b) scaling exponent of a small-world network of HH neurons with $p = 0.001$ as a function of the coupling strength, for $N = 2000$.

For a single neuron a vanishing minimum firing rate is due to the fact that, if r is too small the interspike interval is large, such that the firing rate closely follows the input rate and it is nearly zero. If the coupling strength is very small but nonzero, we expect the same scenario to happen, but if $\bar{g}_c$ increases past a critical value, a kind of synchronization emerges, and the minimum firing rate increases due to a coherent behavior. This leads to a saturation value of $F_{\min}$, as observed in numerical simulations.

The coupling strength $\bar{g}_c$ also affects both the dynamic range [Fig. 6(a)] as well the scaling exponent [Fig. 6(b)]. The latter decreases from ∼0.7 (weakly coupled neurons) to 0.3 for strongly coupled neurons. A possible explanation of this effect follows an inspection of the $F \times r$ curves displayed in Fig. 5(a): as the coupling strength increases the minimum firing rate also increases, whereas the maximum firing rate remains unchanged at 0.2. Therefore the sigmoidal curve tries to accommodate the increase in $F_{\min}$ with fixed $F_{\max}$, and tends to be less steep in the scaling region, i.e. decreasing the scaling exponent.

The dynamic range has a different behavior, though, since it increases as the coupling strength goes from zero to 0.04 mS/cm^2, achieves a maximum value of 20 dB and decreases again to ∼16 dB, yet higher than the value for weak coupling (14 dB). Again we can understand this situation from Fig. 5(a) since, if the coupling is small enough, the curves become different but they must obey $F_{\min} = 0$ nevertheless, what can be accomplished by becoming less steep, so increasing the dynamic range. This explains the increase of Δ observed for weak coupling. However if the coupling strength becomes larger the curves cannot be less steep for a larger interval thanks to the maximum firing rate which is fixed at 0.2. The scaling intervals become shorter, and thus the dynamic range decreases for strong coupling.

The variation of Δ with the network size is displayed in Fig. 7(a). The dynamic range grows monotonically with N from 12 dB, which is the value for a single neuron to a saturation value near 30 dB for large networks. Hence the dynamic range has grown three times its value due solely to the increase of network size. Fig. 7(b) shows the variation of the scaling exponent m with the number of neurons N (provided in all cases we have a small-world connection architecture). It turns out that m, which is ∼0.8 for a single neuron, decreases with N such that, for larger networks the exponent saturates at ∼0.2.

A third parameter which we can vary in the context of small-world models of neuronal networks is the probability p with which new connections are randomly added to the regular one-dimensional chain of nodes. From the results of Section 4, we concluded that $p = 0.01$ (corresponding to just 1% of shortcuts added to the chain) is a value for which the small-world properties are fulfilled. As a matter of fact, a wider range of p-values would give good results as well since it suffices for small-world networks to have "large" values of the merit figure S. This freedom allows one to choose values of p within a wide interval, as long is p is kept small enough.

The relation between F and r is illustrated in Fig. 8(a) by considering different values of p, indicated by different curves, from $p = 0$ (blue points), corresponding not to a small-world but to a regular chain of near-neighbor links, to $p = 0.009$ (red point), a representative example of a small-world network according to our analysis. The sigmoid relationship persists for all considered values of p, with a minimum firing rate $F_{\min}$ increasing with p, what can be best viewed in Fig. 8(b).

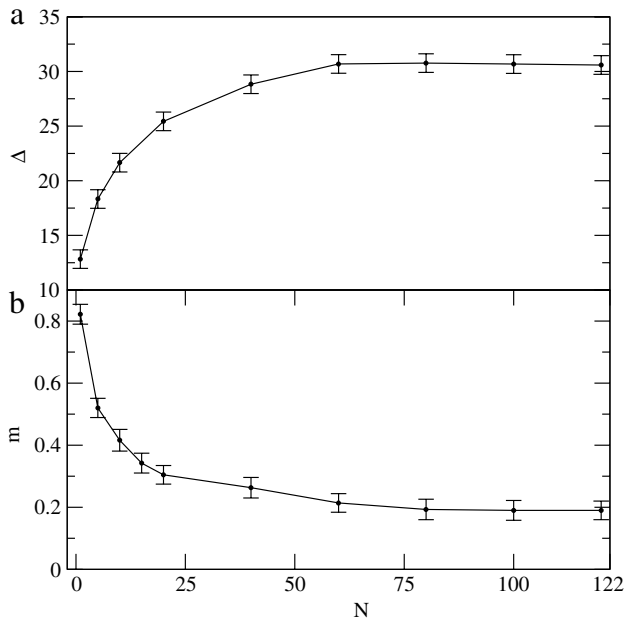

Fig. 7. (a) Dynamic range and (b) exponent of the scaling law $F \sim r^m$ for a small-world network of HH neurons with $p = 0.001$ as a function of the network size, for $\bar{g}_c = 0.06$ mS/cm^2.

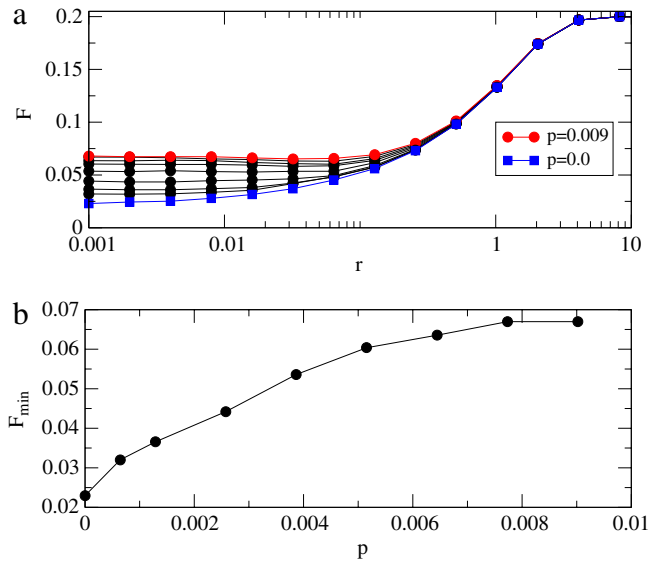

Fig. 8. (a) Firing rate *vs.* spike input rate for various values of the shortcut probability p, from 0.0 (blue line) to 0.009 (red line). (b) Minimum firing rate as a function of p. We considered $\bar{g}_c = 0.06$ mS/cm^2 and $N = 2000$. (For interpretation of the references to color in this figure legend, the reader is referred to the web version of this article.)

The larger is p, the more shortcuts are added to an otherwise regular chain of networks with synapses between near neighbors. The effect of these shortcuts is to introduce nonlocal connections, i.e. spatially distant neurons can be connected by chemical synapses. On the other hand, electric synapses are based in gap junctions that require neurons to be adjacent. Hence, although electric synapses may be important in various models of sensory neurons, we have limited ourselves in this work to chemical synapses. A model using both electric and chemical synapses has been developed on the basis of a cellular automaton [15,16].

The nonlocal shortcuts introduced with increasing p-values have an overall effect similar to the increase of the coupling strength: as an example, instead of augmenting the conductance of a single synapse, the effect of two synapses would give the same result. Based on this reasoning, we expect that the increase of p would be similar to the increase of $\bar{g}_c$ [Fig. 5].

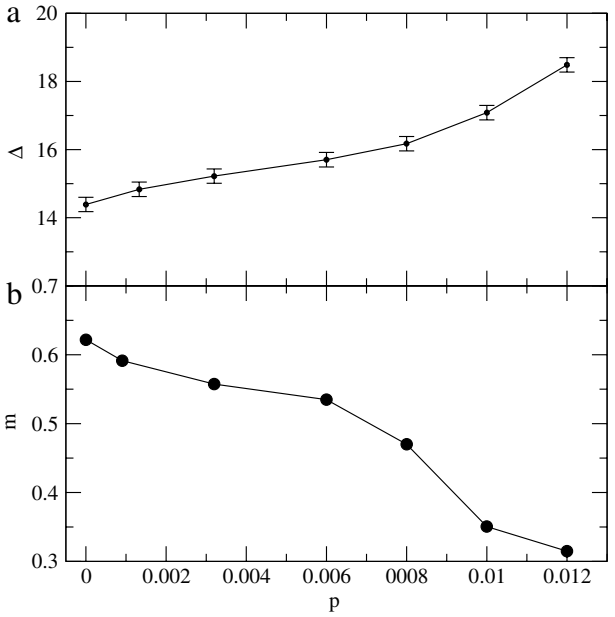

Fig. 9. (a) Dynamic range and (b) scaling exponent of a small-world network of HH neurons with $\tilde{g}_c = 0.03$ mS/cm^2 as a function of the shortcut probability, for $N = 2000$.

Indeed we have an increase of the dynamic range as the probability p increases from 0 (a pure regular chain) to 0.012 (a small-world network) [Fig. 9(a)] and a decrease of the scaling exponent [Fig. 9(b)]. The dynamic range goes from 14 dB, in a region where we do not have small-world property, to ∼18 dB along the whole interval where our network can be considered a small-world one. On the contrary, the scaling exponent appears not to saturate for larger p. Hence, although we can assign a common value of Δ for a small-world network, the value of m seems to be strongly dependent on the fraction of nonlocal shortcuts.

Note that the dynamic range has increased only ∼4 dB by increasing the probability of nonlocal shortcuts. This is in sharp contrast with the increase of ∼18 dB observed when we add neurons to the network [Fig. 7(a)]. When we vary the probability p of nonlocal shortcuts, since p is small, for the network sizes we have used in numerical simulations, the maximum number of shortcuts added to the ring with local connection is about 20. This effect is, in fact, much smaller than what is obtained by increasing the network size since, for each neuron added to the lattice, we expect to add at least $2\ell = 4$ local connections and perhaps one (at most) nonlocal shortcuts. Hence the effect of increasing network size is indeed more important than the increase of the probability of nonlocal shortcuts.

We close this Section by making a comparison between our main results and the ones previously obtained by other authors and previous work of the present authors. Kinouchi and Copelli have considered the problem of dynamic range using deterministic cellular automaton models where the state variable has n states: $s = 0$ is the resting state, $s = 1$ is the active state, and the remaining $n - 2$ are refractory states [12]. In this model there have been considered random (ER) networks with a variable probability, and the relevant control parameter used in this study was the average branching ratio σ of the network. They found that the dynamic range increases with the average branching ratio from ∼17 to ∼26 dB at a critical point $\sigma = 1$ and then decreases again (cf. Fig. 2(d) of Ref. [12]). Our investigation, on the other hand, considers a small-world network topology, which is based on a regular chain in which nonlocal shortcuts are randomly introduced with a given probability. Although the average path length of a small-world network is comparable to a random one, the clustering coefficient is much larger, then the statistical properties of SW networks are expected to be quite different from the ER case.

However, the variation of the dynamical range with the synaptic conductance, which plays the role of coupling strength [see Fig. 6(a)] reveals an interesting analogue with the results of Kinouchi and Copelli, since the dynamic range increases from ∼14 dB to a maximum of ∼20 dB as the coupling strength increases, and decreases afterwards, in the same fashion it does in the Kinouchi and Copelli's work, where the average branching ratio plays a role similar to the coupling strength in our work. Hence, on the basis of such analogy, we can guess that the behavior we observed in Fig. 6(a) may be interpreted as the existence of an optimal dynamic range with respect to variations in coupling strength.

In a previous work of the present authors, a modification of the Kinouchi and Copelli model was proposed, in which nonlocal shortcuts were introduced in the cellular automaton to play the role of chemical synapses, assuming that the local connections stand for electric, or gap junction synapses [16]. In that case the varying parameters were the probability of nonlocal shortcuts p and the time delay τ. We found that the dynamic range increases from ∼35 to ∼55 dB as the probability increases, and stays nearly constant at ∼55 dB as long as the time delay is not too large. In the present work we also observed

an increase of the dynamic range with the probability of nonlocal connections [cf. Fig. 9(a)], but the scale of probabilities is somewhat different, since the model of Ref. [16] is not meant to describe a small-world network.

6. Conclusions

The dynamic range measures the interval of response of a neural system, in presence of stimuli of varying intensity. Within this range, Stevens' law prescribes a power-law scaling for the stimulus–response relationship. For a neural system we mean, at the microscopic level, a single neuron and, at the macroscopic level, a neuronal network, which can be directly related to a sensory organ. Previous results obtained with neurocomputational models indicate that in both levels Stevens's law is valid, although with different values of both the dynamic range and the scaling exponent. The dynamic range of a single neuron is substantially less than the range of a sensory organ, suggesting that the enhancement of the dynamic range may be a collective effect of the neuronal network structure.

In this work we aimed to investigate the factors that would affect the dynamic range and the scaling exponent. For that we consider a computer model of a neuronal network, in which individual neurons are described by Hodgkin–Huxley equations, and a small-world network of neurons connected by chemical synapses. The small-world network has been constructed by randomly adding nonlocal shortcuts with a given probability to a one-dimensional chain of networks with local connections.

The external inputs were chosen to be stereotyped point events with intervals distributed according to a Poisson process of given input rate, which measures the intensity of the stimulus. The intensity of the response is measured by the firing rate of the coupled neurons. We verified that a sigmoidal relation holds between the intensities of the stimuli and response for different values of the coupling strength and the shortcut probability.

In the core of these sigmoidal relations there is a power-law scaling with a given exponent, and the dynamic range measures the extent of this scaling region. We verified that the dynamic range increases with the number of neurons, from a value near 10 dB for isolated neurons, to a value *circa* 30 dB for large networks. The scaling exponent diminishes with the network size and saturates at $\sim$0.2.

The maximum firing rate does not vary with any of these parameters, since it is related to the duration of the refractory period of each neuron, whose model parameters are kept fixed. The minimum firing rate, on the other hand, was found to increase with both coupling strength and probability. In the former case, the increase has features of a continuous phase transition, that may be related to a synchronized behavior in the phases of spiking events.

The increase of the minimum firing rate, jointly with the constraint of keeping the maximum firing rate at a fixed value, affects both the dynamic range and the scaling exponent, as the coupling parameters are varied. The dynamic range seems to stabilize at a value of $\sim$16 dB for large coupling strengths, after achieving a local maximum of 20 dB. The scaling exponent, on the other hand, saturates at $\sim$0.3 for strongly coupled networks. Similar conclusions are drawn when the probability of nonlocal shortcuts is increased towards 0.01, a suitable value for a small-world network. Those results compare well with values of the dynamic range and scaling exponents for sensory organs. For example, the dynamic range of the glomeruli is $\sim$30 dB, which is three times the dynamic range ($\sim$10 dB) of single olphatory receptor neurons [43,44].

Our approach permitted a more detailed investigation than what could be done with a cellular automaton, where the number of variable parameters is more limited. Nevertheless, although the neuronal dynamics model is realistic enough, the connection architecture we have used is somewhat simplified. Complex networks have a modular structure, like the functional network of the cat brain, demanding the use of more sophisticated methods, like clustered networks. This is a natural extension of the present work, but results are more difficult to obtain due to limitations of computer memory and CPU time.

Another factor that we shall take into account in future numerical simulations is that, in the present work, we limited ourselves to excitatory synapses only. This choice has been made so as to reduce the number of variable parameters. We are also considering simulations with balanced random network models, in which excitatory and inhibitory synaptic conductances are roughly equal and neurons operate in a fluctuation-driven regime [45,46].

Acknowledgments

This work was made possible through partial financial support from the following Brazilian research agencies: CNPq (grant no. 552148/2011-3) and CAPES (grant no. 17656-12-5) (Procad). The computer simulations were performed at the LCPAD cluster at Universidade Federal do Paraná, acquired from the financial support provided by FINEP (CT-INFRA). We acknowledge useful discussions with K. Iarosz.

References

[1] S.S. Stevens, in: G. Stevens (Ed.), Psychophysics: Introduction to its Perceptual, Neural and Social Prospects, Wiley, New York, 1975.
[2] L.E. Krueger, Behav. Brain Sci. 12 (1989) 251.
[3] G.M. Siegel, E.J. Schork Jr, H.L. Pick Jr, S.R. Garter, J. Speech Hear. Res. 25 (1982) 473.
[4] J.-P. Rospars, P. Lánský, P. Ducmap-Viret, A. Duchamp, Biosystems 58 (2000) 133.
[5] J.-P. Rospars, P. Lánský, P. Ducmap-Viret, A. Duchamp, Eur. J. Neurosci. 18 (2003) 1135.
[6] T.A. Cleland, C. Linster, Neural Comput. 11 (1999) 1673.
[7] K.J. Kim, F. Rieke, J. Neurosci. 23 (2003) 1506.

[8] M.R. Deans, B. Volgyi, D.A. Goodenough, S.A. Bloomfield, D.L. Paul, Neuron 36 (2002) 703.
[9] K.M. Dorries, J.S. Kauer, J. Neurophysiol. 83 (2000) 754.
[10] D.-Q. Zhang, D.G. McMahon, Proc. Natl. Acad. Sci. USA 97 (2000) 14 754.
[11] M. Copelli, A.C. Roque, R.F. Oliveira, O. Kinouchi, Phys. Rev. E 65 (2002) 060901. (R).
[12] O. Kinouchi, M. Copelli, Nat. Phys. 2 (2006) 348.
[13] D.R. Chialvo, Nat. Phys. 2 (2006) 301.
[14] V.R.V. Assis, M. Copelli, Phys. Rev. E 77 (2008) 011923.
[15] K.C. Iarosz, A.M. Batista, R.L. Viana, S.R. Lopes, I.L. Caldas, T.J.P. Penna, Physica A 391 (2012) 819.
[16] R.L. Viana, F.S. Borges, K.C. Iarosz, A.M. Batista, S.R. Lopes, I.L. Caldas, Commun. Nonlinear Sci. Numer. Simul. 19 (2014) 164.
[17] A.L. Hodgkin, A.F. Huxley, J. Physiology 117 (1952) 500.
[18] D.S. Bassett, E. Bullmore, Neuroscientist 12 (2006) 512.
[19] C.L. Buckley, T. Nowotny, Phys. Rev. Lett. 106 (2011) 238109.
[20] J.R. Clay, D. Paydaffar, D.B. Forger, J. Roy. Soc. Interface 5 (2008) 1421.
[21] A. Destexhe, Z.F. Mainen, T.J. Sejnowski, Neural Comput. 6 (1994) 14.
[22] Y. Hao, Y. Gong, L. Wang, X. Ma, C. Yang, Chaos Solitons Fractals 44 (2011) 260.
[23] A. Kern, R. Stoop, Phys. Rev. Lett. 91 (2003) 128101.
[24] W. Gerstner, A.K. Kreiter, H. Markram, A.V. Herz, PNAS 94 (1997) 12740.
[25] M. Meister, M.J. Berry II, Neuron 22 (1999) 435.
[26] M. Levine, J.M. Shefner, Biophys. J. 19 (1977) 241.
[27] W. Bair, C. Koch, W. Newson, K. Britten, J. Neurosci. 14 (1994) 2870.
[28] R. Brette, M. Rudolph, T. Carnevale, M. Hines, D. Beeman, J.M. Bower, M. Diesmann, A. Morrison, P.H. Goodman, F.C. Harris Jr., M. Zirpe, T. Natschläger, D. Pecevski, B. Ermentrout, M. Djurfeldt, A. Lansner, O. Rochel, T. Vieville, E. Muller, A.P. Davison, S. El Boustani, A. Destexhe, J. Comput. Neurosci. 23 (2003) 349.
[29] W. Gerstner, W.M. Kistler, Spiking Neuron Models, Cambridge University Press, 2002.
[30] E.R. Kandel, J.H. Schwartz, T.M. Jessell, Principles of Neural Science, fourth ed., McGraw-Hill, 2000.
[31] J.W. Scannell, M.P. Young, Curr. Biol. 3 (1993) 191.
[32] D.J. Watts, Small Worlds, Princeton University Press, Princeton, 2000.
[33] R. Albert, A.-L. Barabási, Rev. Modern Phys. 74 (2002) 47.
[34] M.E.J. Newman, D.J. Watts, Phys. Lett. A 263 (1999) 341.
[35] P. Erdös, A. Rényi, Publ. Math. 6 (1959) 290.
[36] D.J. Watts, S.H. Strogatz, Nature 393 (1998) 409.
[37] M.D. Humphries, K. Gurney, PLOS One 3 (2008) e0002051.
[38] L.R. Varshney, B.L. Chen, E. Paniagua, D.H. Hall, D.B. Chklovskii, PLOS Comput. Biol. 7 (2011) e1001066.
[39] O. Sporns, J.D. Zwi, Neuroinformatics 2 (2004) 145.
[40] C.C. Hilgetag, G.A. Burns, M. O'Neill, J.W. Scannell, M.P. Young, Philos. Trans. R. Soc. Lond. B, Biol. Sci. 355 (2000) 91.
[41] C.C. Hilgetag, M. Kaiser, Neuroinformatics 2 (2004) 353.
[42] J.W. Scannell, C. Blakemore, M.P. Young, J. Neurosci. 15 (1995) 1463.
[43] M. Wachowiak, L.B. Cohen, Neuron 32 (2001) 723.
[44] H.U. Fried, S.H. Fuss, S.I. Korsching, Proc. Natl. Acad. Sci. USA 99 (2002) 3222.
[45] N. Brunel, J. Comput. Neurosci. 8 (2000) 183.
[46] A. Kuhn, A. Aertsen, S. Rotter, J. Neurosci. 24 (2004) 2345.